RSC Advances

ROYAL SOCIETY OF CHEMISTRY

www.rsc.org/advances

Two-step dielectric anomalies coupled with structural phase transitions in co-crystal of 1,4-diazabicyclo[2.2.2]octane and 4, 4'-biphenol

Wei-Hua Ning,[a,b] Lu Zhai[a,b] and Xiao-Ming Ren*[a,b,c]

[a] State Key Laboratory of Materials-Oriented Chemical Engineering and College of Science, Nanjing University of Technology, Nanjing 210009

[b] College of Materials Science and Engineering, Nanjing University of Technology, Nanjing 210009

[c] Coordination Chemistry Institute & State Key Laboratory, Nanjing University, Nanjing 210093

Tel.: +86 25 58139476

Fax: +86 25 58139481

Email: xmren@njtech.edu.cn

Abstract

The co-crystal of 4, 4'-biphenol with 1, 4-diazabicyclo[2.2.2]octane (**1**) was obtained using mutual diffusion approach of two components methanol solution at ambient temperature. DSC measurement detected that **1** undergoes two reversible phase transitions at 182 K/167 K and 236 K/229 K in heating/cooling cycle. The phases are named: high-temperature (HT), intermediate (IT) and low-temperature (LT) ones in descending order of temperature. Each reversible phase transition corresponds to a dielectric anomaly, respectively. The single crystal structure analysis revealed that an isostructural phase transition occurs between HT and IT phases while a symmetry-breaking structural phase transition undergoes between IT and LT phases.

Keywords: Co-crystal, order–disorder transformation, structural phase transition, dielectric anomaly

Introduction

Phase transitions in materials occur widely in nature and can often impart functionality to the system, sometimes leading to important technological innovations. The physical properties of a material may change massively across a solid-to-solid phase transition.[1-4] For example, vanadium dioxide (VO_2) undergoes a metal-to-insulator (MI) transition at 341 K and shows dramatic changes in electrical resistivity and infrared transmission across this phase transition.[5,6] An organic molecular conductor, based on a spiro-biphenalenyl neutral radical, goes through a structural phase transition near room temperature and simultaneously exhibits bistability in electrical, optical and magnetic properties.[7] The material that undergoes fast and reversible phase transition is very useful in practical applications.[1-8]

The dielectric phase transition is one of the most attractive features of material since the conversion between the distinct high and low dielectric states has succeeded in photoelectronic fields. A lot of progress has been achieved in designing solid state dielectrics,[9, 10] however, the main challenge how to get two or more obviously different dielectric states is still for dielectric materials. As one of the most promising strategies to assemble such a functional material, usually, to design and synthesize molecule compounds with structural transformations effectively acquires the typically temperature-dependent dielectric states.[10, 11] The order-disorder transformation in crystal generally induces the dielectric phase transition,[12-17] this is due to that the dielectric permittivity of a material depends on its density and total polarizability of molecules and the change of molecule arrangements probably leads to the variation of total polarizability of molecules. We noted that several 1,4-diazabicyclo[2.2.2]octane (abbr. DABCO) compounds show structural disorder in their crystals, among them, the [DABCO][$HClO_4$], [DABCO][HBF_4] and [DABCO][$HReO_4$] crystals showed ferroelectric behavior,[18,19] while [DABCO][HBr] and [DABCO][HI] crystals exhibited unique anisotropic ferroelectric-relaxor properties.[20-22] owing to the disorder-to-order transformation of DABCO molecules. Ferguson et al. reported the

crystal structure of 4, 4'-biphenol and DABCO co-crystal at ambient temperature fifteen years ago,[23] which indicated DABCO molecule in this co-crystal exhibiting displacively disordered. It is expected that the dynamically disordered DABCO molecules at ambient temperature may be frozen to form an ordered structure in low temperature.

In this study, we measured the temperature dependent dielectric permittivity in the temperature ranges of 123-353 K, and found that the co-crystal shows two-step anomalies in dielectric spectroscopy. We further investigated the crystal structures of this co-crystal at selected temperature, which revealed that the dielectric anomalies are respectively coupled to the isostructural phase transition and symmetry breaking structural phase transition as well.

Experimental section

Chemicals, materials and preparation of co-crystal (1)

All chemical reagents were used without further purification. Co-crystal **1** was prepared by a slow diffusion procedure at ambient temperature: the 4, 4'-biphenol and DABCO with molar ratio of 1:1 were respectively dissolved in methanol, the saturated methanol solution with 1, 4-Diazabicyclo[2.2.2]octane was placed at the bottom of a test tube and the dilute methanol solution with 4, 4'-biphenol was carefully to be added at the top of the methanol solution with 1, 4-diazabicyclo[2.2.2]octane, and the block-shaped crystals were obtained over seven days. The crystals were collected by filtration, which are suitable for the single crystal x-ray diffraction.

Elemental microanalysis calculated for $C_{18}H_{22}N_2O_2$ (**1**): C, 72.46; H, 7.43; N, 9.39%. Found: C, 72.45; H, 7.21; N, 9.12%. IR spectrum (KBr pellet, cm^{-1}) and the assignments for the listed bands: 3420(vw) attributed to the ν_{O-H} of the 4, 4'-biphenol; 3052(w) and 3026(w) attributed to the ν_{C-H} of the phenyl ring; 2973(w), 2942(s), 2876(s) attributed to the ν_{C-H} of DABCO; 1608(m), 1589(s), 1503(s), 1459(s) attributed to the ring stretching vibration of the phenyl of the 4, 4'-biphenol; 1388(w), 1354(w) attributed to the δ_{C-H} in the DABCO; 1268(s) arose from the ν_{C-N} of the

DABCO; 1243(s) arose from the ν_{C-O} of the 4, 4'-biphenol; 1169(s) arose from the ν_{C-C} of the DABCO; 782(s) attributed to γ_{-CH2-} of DABCO.

Physical measurements

Elemental analyses (C, H and N) were performed using an Elementar Vario EL III analytical instrument. Infrared (IR) spectrum was recorded on a Bruker VERTEX80V Fourier transform infrared spectrometer (KBr disc) at room temperature under vacuum. Powder X-ray diffraction (PXRD) data were collected on a Bruker D8 Advance powder diffractometer, operated at 40 kV and 40 mA, with Cu Kα radiation (λ = 1.5418 Å), and the measurement was perform at ambient temperature in the range 2θ = 5-50° with 0.02 °/step and 1.2 s/step. Differential scanning calorimetry (DSC) were carried out on a Q2000 V24.9 Build 121 instrument over the temperature range from −180 to 20 °C (93–293 K) at a heating rate of 20 °C·min^{-1}. Temperature- and frequency-dependent dielectric permittivity (ε') and dielectric loss *tan(δ)* were measured using a Concept 80 system (Novocontrol, Germany) between −150 and 80 °C (123–353 K) and ac electric field frequencies span from 10^2 to 10^7 Hz. A selected block-shaped single crystal, with dimensions 2.00 mm × 2.00 mm × 1.50 mm, was used for the dielectric measurement, where the conducting silver paste was coated on the two opposing surfaces (2.00 mm × 2.00 mm) of the single crystal, and gold wires (80 μm diameter) were utilized to connect the copper electrodes and the single crystal surfaces.

X-ray single crystallography

The single-crystal X-ray diffraction data were collected at 120 K, 200 K, 296 K with graphite monochromated Mo Kα (λ = 0.71073 Å) on a CCD area detector (Bruker-SMART) for **1**. Data reductions and absorption corrections were performed with the SAINT and SADABS software packages,[24] respectively. Structures were solved by direct method using the SHELXL-97 software package.[25] The non-hydrogen atoms were anisotropically refined using the full-matrix least-squares method on F^2. The hydrogen atoms in the OH groups of 4, 4'-biphenol were found

from Difference Fourier Map, and all hydrogen atoms, besides those in the OH groups, were placed at the calculated positions and refined riding on the parent atoms for the structures at 120 K, 200 K, 296 K. The details about data collection, structure refinement and crystallography are summarized in Table 1.

Results and discussion

DSC measurement and Dielectric property

DSC plot of **1** in the temperature range 125-275 K is depicted in Figure 1, which clearly demonstrates two thermal anomalies appeared at ca. 182 K/167 K and ca. 236 K/229 K upon heating/cooling, respectively. For convenience, the phase is sequentially named as the high-temperature (HT), intermediate (IT) and low-temperature (LT) ones in order of decreasing temperature. The ΔH and ΔS (ΔS = ΔH/Tc;[26] T_C represents the critical temperature of phase transition) values of phase transition were estimated to be 158.9 J/mol and 0.87 $J \cdot mol^{-1} \cdot K^{-1}$ from LT to IT phase transition as well as 189.6 J/mol and 0.80 $J \cdot mol^{-1} \cdot K^{-1}$ from IT to HT phase transition, respectively. The entropy differences ΔS between two phases (phase 1 and phase 2) can be expressed as the equation 1 in statistical mechanics,

$$\Delta S = R \ln \frac{\Omega_1}{\Omega_2} \qquad (1)$$

Where R(= 8.31 $J \cdot K^{-1} \cdot mol^{-1}$) is the gas constant, Ω_i (i = 1 and 2) represent the state numbers in phases 1 and 2, respectively. The values of Ω_{HT}/Ω_{IT} and Ω_{IT}/Ω_{LT} were estimated to be 1.1 and 1.11, indicating that the state numbers between HT and IT as well as between IT and LT are the almost same. This conclusion is further confirmed by the single crystal structure analyses for **1** in HT, IT and LT phases (see next section).

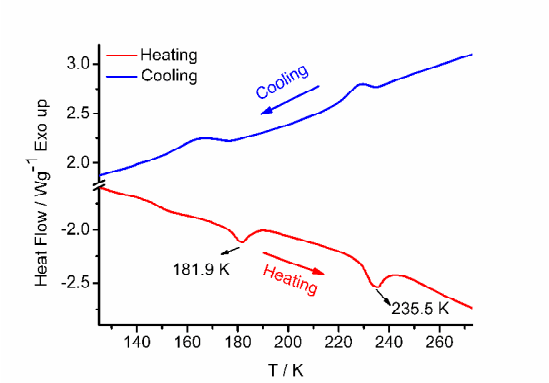

Figure 1 DSC plots of **1** showing two thermal anomalies in the temperature range 160-240 K.

The temperature dependent dielectric permittivity was investigated in the temperature ranges of 123-353 K and within the frequency regimes of 1-10^7 Hz. As displayed in Figure 2a, a broad and asymmetric dielectric anomaly peak occurs in the temperature interval of 140-300 K in the plots of ε' versus T at the selected frequencies. Obviously, the broad peak is comprised of two overlapped peaks. Thus, the multiple peaks fitting approach, with two Gaussian-type profiles, was used to separate the overlapped peaks in the temperature range 140-300 K at f = 10^2 Hz (see Figure 2b), giving two maximum around 190 K and 220 K, and these temperatures correspond well to the phase transition temperature determined by DSC measurements (ref. Figure 1). It was noted that the dielectric permittivity is ca. 62 in LT phase (below 140 K) and ca. 58 in HT phase (above 240 K), respectively, and these values are close to each other.

The dielectric permittivity of a material is a complex function and depends on the density and total polarizability of the molecules in crystal. Various factors contribute to the polarizability of a material, such as space-charge polarization, dipolar interactions, atomic, ionic, distortions and electronic interactions. Thus, a dielectric anomaly is probably a result of crystal structure change. And then we investigated the crystal structures at 120 K in LT phase, 200 K in IT phase and 296 K in HT phase.

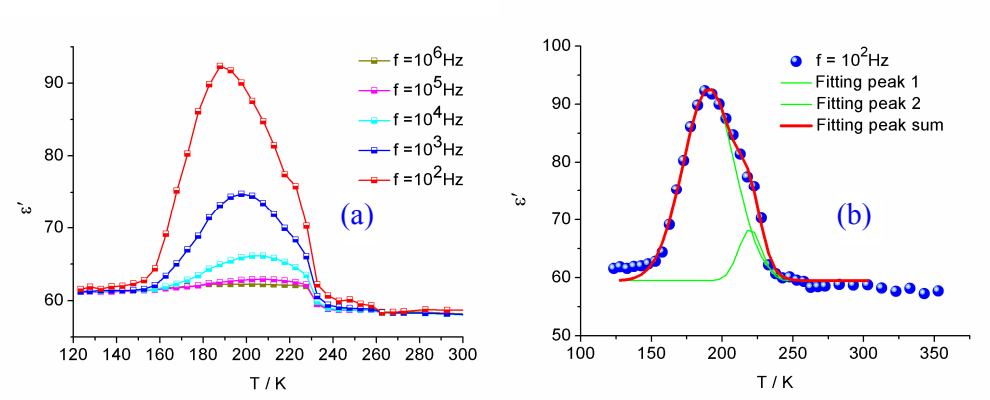

Figure 2 (a) Plots of dielectric permittivity versus temperature over the range 123-353 K and within frequency regions 10^2-10^6 Hz (b) two Gaussian-type profiles was used to fit the dielectric permittivity in the temperature range 140-300 K at f = 10^2 Hz.

Crystal structure changes across phase transitions

The crystal structure of **1** in HT phase was previously reported in the literature,[23] for convenient comparison of structural changes in different phases, we descript simply the crystal structure of **1** in HT phase.

Co-crystal **1** crystallizes in the centrosymmetric space group *C2/c* in HT phase. As displayed in Figure 3a, an asymmetric unit of **1** is comprised of one half 4, 4'-biphenol molecule together with one half DABCO molecule. The DABCO molecule shows dynamically disorder, and the principal effect of the disorder is the switching of the two nitrogen sites, with only a slight positional displacement ($d_{N1...N2}$ = 0.145(22) Å). It is worth noting that two disorder DABCO molecules are related to each other via an inversion center, thus, the site occupied factor is 0.5 for all atoms in DABCO. The 4, 4'-biphenol molecule adopts non-planar conformation where two phenyl rings are twisted to each other with a dihedral angle 39.9°; this molecule possesses C_2 point group symmetry, the twofold rotation axis passes through the midpoint of the C4-C4#1 bond (symmetric code #1 = 1-x, y, 0.5-z) and is parallel to the *b*-axis. The bond parameters in both DABCO and 4, 4'-biphenol molecules, listed in Table S1, fall within the expected ranges and are similar to those reported in the literature.[23] As shown in Figure 3c, the DABCO and 4, 4'-biphenol molecules are arranged into

alternating molecule layers, and such molecule layers are parallel to the crystallographic (0 0 1) plane. There are strong intermolecular H-bonds between the neighboring DABCO and 4, 4'-biphenol molecule layers, with H-bond parameters of ∠O1-H1…N1 = 166.6° and $d_{O1\ldots N1}$ = 2.771(13) Å versus ∠O1-H1…N2 = 164.5° and $d_{O1\ldots N2}$ = 2.651(19) Å, which connect the DABCO and 4, 4'-biphenol molecules to form a wave-shaped supramolecular chain along a+c/2 direction (see Figure 3c).

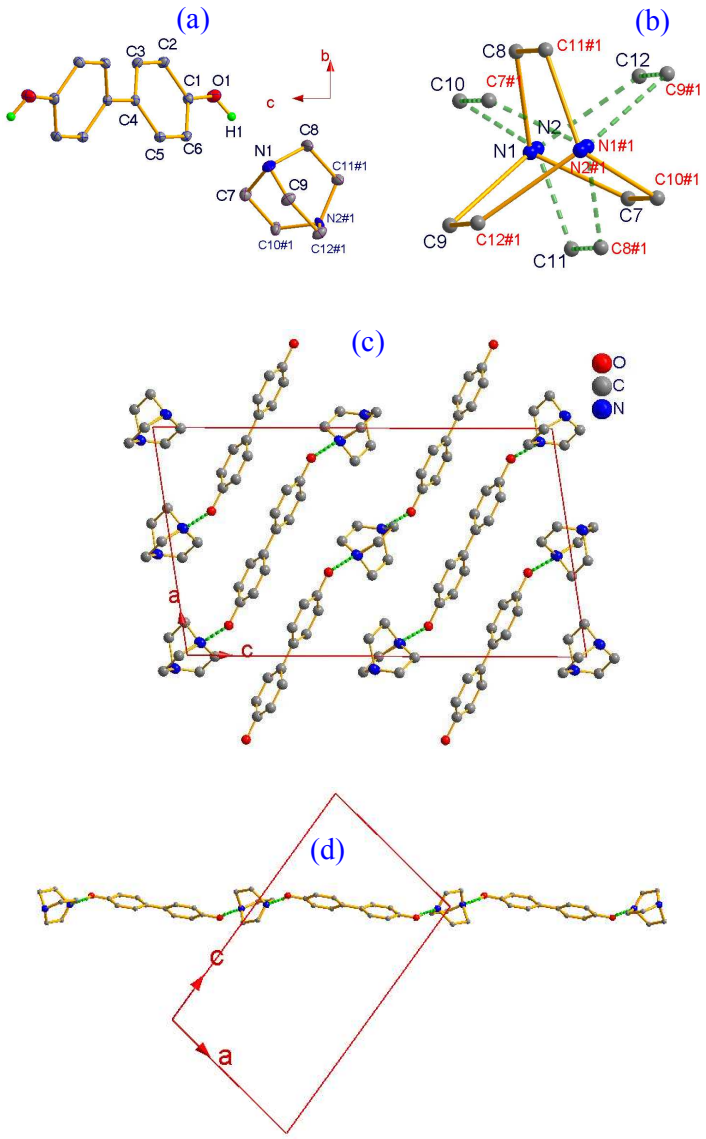

Figure 3 (a) Molecular structure of **1** with non-hydrogen atoms labeling and displacement ellipsoids at the 10% probability level in HT phase, where hydrogen atoms besides in OH groups as well as one disordered BADCO molecule are omitted

for clarity (b) the disordered BADCO molecule with two different orientations related to each other via an inversion center (c) packing structure viewed along b-axis (d) one-dimensional H-bond chain along a+c/2 direction.

The IT phase is isostructural to the HT one. These two phases show quite similar lattice parameters and packing structure. The transition between HT and IT phases is accompanied by change in neither the crystallographic space group nor the occupied Wyckoff positions. Such a transition has been categorized as "isostructural phase transition" (IPT), which is also known as "Cowley's type zero" transitions[27] after Cowley postulated the possibility of such a transition, based on the behavior of acoustic phonons within the framework of displacively structural phase transitions. Consequently, the intermolecular distances and the relative orientation between the neighboring DABCO and 4, 4'-biphenol molecules were carefully inspected. The positional displacement of the switched two nitrogen sites $d_{N1\ldots N2}$ = 0.458 Å, which is more than two times the value in HT phase. The characteristic angles are schematically illustrated in Figure 4, where line L1 passes through the C–C bond connected two phenyl rings of 4, 4'-biphenol molecule; line L2/L3 represents line passing through two N atoms in DABCO molecule. The angles θ1, θ2, and θ3 as well as the geometric parameters of intermolecular H-bonds between DABCO and 4, 4'-biphenol molecules in HT and IT phase are summarized in Table 2, indicating that θ1, θ2, and θ3 as well as the distances $d_{O\ldots N}$ and $d_{H\ldots N}$ are almost the same in HT and IT phases while the angle ∠O1-H1…N2 increases by 6.7° and ∠O1-H1…N1 reduces by 7.3° from HT to IT phase.

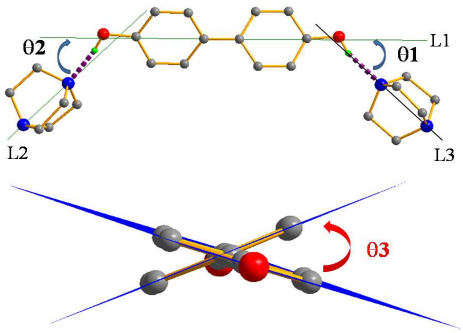

Figure 4 Schematic illustration of the characteristic angles (θ1 and θ2: the angles between the lines L1 and L2/L3; θ3: dihedral angle between two phenyl rings in 4, 4'-biphenol).

From the IT to LT phase, the space group of co-crystal **1** changes from monoclinic *C2/c* to monoclinic $P2_1/c$, the asymmetric unit switches from one half DABCO together with one half 4, 4'-biphenol molecule to one DABCO together with one 4, 4'-biphenol molecules. In addition to these changes, the disorder DABCO molecule in IT phase becomes frozen in LT phase and the 4, 4'-biphenol molecule lost the C_2 point group symmetry (ref. Figure S5). Thus, the transition between the IT and LT phases is categorized as a symmetry breaking structural phase transition. The bond parameters in both DABCO and 4, 4'-biphenol molecules, summarized in Table S1, are comparable to those in both IT and HT phases, and the packing structure is also analogous to those in IT and HT phases. The characteristic angles related to the relative orientation between the DABCO and 4, 4'-biphenol molecules and the parameters of intermolecular H-bonds, summarized in Table 2, are close to those in IT phase, for example, the largest changing angle θ2 only decreases by ca. 2.0° from IT to LT phase.

Temperature-dependent cell dimensions (axes and volumes) were further examined to investigate the structural change with temperature in HT, IT and LT phases, the axes and volumes as a function of temperature in the interval between 120 and 296 K are displayed in Figure 5. It was noted that there exist three different linearly behaviors in the different temperature regions, above 225 K, between 175 and 225 K as well as below 225 K, which correspond to the HT, IT and LT, respectively. The cell dimensions show distinct behavior of thermal variation between HT and IT phases although two phases are isostructural. As temperature decreases, the *b*- and *c*-axes and cell volume V reduce while the *a*-axis expands (the length of *a*-axis increases by ca. 1% between 296 and 225 K) in HT phase, while the *a*-axis and cell volume V reduce, the *b*-axis remains almost unchanged, while the *c*-axis expands in IT phase. As shown in Figure 5, the length of *a*-axis decreases by ca. 8% and the

length of c-axis raises by ca. 4% between 175 and 225 K in IT phase. The variations of cell dimensions in both HT and LT phases correspond to the changes of the relative orientation as well as the intermolecular separations between DABCO and 4, 4'-biphenol molecules. The cell dimensions are almost temperature independent in the ordered LT phase.

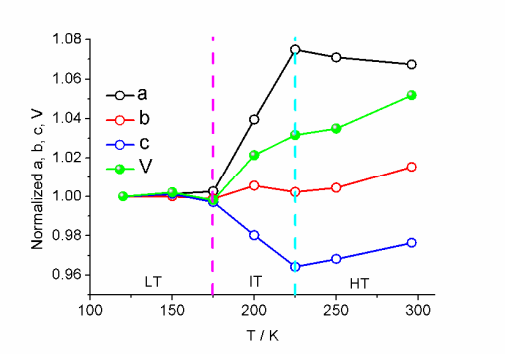

Figure 5 Temperature-dependent cell dimensions (axes and volumes) for **1**, all under the low temperature cell settings, and normalized over the dimensions at the lowest temperature points.

Crystal structure changes and dielectric anomaly

The electric polarizability is the tendency of a material to allow an externally applied electric field to induce electric dipoles (separated positive and negative charges) in the material. Polarization P is related to the electric field E and the electric displacement D by

$D = \varepsilon_0 E + P$ (2)

Where P is related to E through χ_e the electric susceptibility of the dielectric $P = \varepsilon_o \chi_e E$. Therefore

$D = \varepsilon_o(1+ \chi_e)E = \varepsilon_0 \varepsilon_r E$ (3)

$P = \varepsilon_0(\varepsilon_r - 1)E$ (4)

Where ε_0 and ε_r represent the permittivity of the free space and the relative dielectric constant of a material. It is noted that P also is the density of atomic electric dipole per unit volume

$P = \Sigma p/V = Np$ (5)

Therefore

$Np = \varepsilon_0(\varepsilon_r-1)E$ (6)

Where p is the dipole moment and N is the density of dipoles. As mentioned above, the ε_r of a material is related to the dipole moment, which depends on the crystal structure. As a result, the structural phase transition probably leads to dielectric anomaly.

Conclusion

In summary, two-step dielectric anomalies were observed at ca. 182 K/167 K and ca. 236 K/229 K upon heating/cooling in the co-crystal of 4, 4'-biphenol with 1, 4-diazabicyclo[2.2.2]octane (**1**). In addition to the dielectric anomalies, the values of dielectric permittivity are similar to each other in HT and LT phases. Single crystal structure analyses disclosed that the isostructural phase transition and the symmetry breaking structural phase transition result in two anomalies in dielectric spectroscopy of **1**, respectively; and the quite analogous packing structures lead to the existence of the comparable dielectric permittivity values in HT and LT phase.

Acknowledgement

The authors thank the Priority Academic Program Development of Jiangsu Higher Education Institutions and National Nature Science Foundation of China for financial support (grant no. 91122011 and 21271103).

Supporting materials

Crystallographic data is available in CIF format for **1** at 120 K and 200 K, in PDF format, are available free of charge via the Internet at ???.

Notes and References

1. Kahn, C.J. Martinez, *Science* 1998, **279**, 44.
2. T. Liu, D.P. Dong, S. Kanegawa, S. Kang, O. Sato, Y. Shiota, K. Yoshizawa, S. Hayami, S. Wu, C. He, C.Y. Duan, *Angew. Chem. Int. Ed.* 2012, **51**, 4367.
3. W. Fujita, K. Awaga, *Science* 1999, **286**, 261.
4. J.A. Koza, Z. He, A.S. Miller, J.A. Switzer, *Chem. Mater.* 2011, **23**, 4105.
5. C.Z. Wu, J. Dai, X.D. Zhang, J.L. Yang, Y. Xie, *J. Am. Chem. Soc.* 2009, **131**, 7218.
6. Y. Muraoka, Z. Hiroi, *Appl. Phys. Lett.* 2002, **80**, 583.
7. M.E. Itkis, X. Chi, A.W. Cordes, R.C. Haddon, *Science* 2002, **296**, 1443.
8. X. Y. Dong, B. Li, B. B. Ma, S. J. Li, M. M. Dong, Y.Y. Zhu, S. Q. Zang, Y. Song, H. W. Hou, T. C. W. Mak, *J. Am. Chem. Soc.* 2013, **135**, 10214.
9. S. Horiuchi, F. Ishii, R. Kumai, Y. Okimoto, H. Tachibana, N. Nagaosa, Y. Tokura, *Nat. Mater.* 2005, **4**, 163.
10. S. Horiuchi, Y. Tokura, *Nat. Mater.* 2008, **7**, 357.
11. T. Akutagawa, S. Takeda, T. Hasegawa, T. Nakamura, *J. Am. Chem. Soc.* 2004, **126**, 291.
12. W. Zhang, Y. Cai, R.G. Xiong, H. Yoshikawa, K. Awaga, *Angew. Chem. Int. Ed.* 2010, **122**, 6758.
13. D.W. Fu, W. Zhang, H.L. Cai, J.Z. Ge , Y. Zhang, R.G. Xiong, *Adv. Mater.* 2011, **23**, 5658.
14. S. Horiuchi, Y. Tokunaga, G. Giovannetti, S. Picozzi, H. Itoh, R. Shimano, R. Kumai, Y. Tokura, *Nature* 2010, **463**, 789.
15. S. Horiuchi, F. Kagawa, K. Hatahara, Y. Tokura, *Nature Comm.* 2012, **3**, 1308.
16. R. Shang, G.C. Xu, Z.M. Wang, S. Gao, *Chem. Eur. J.* 2014, **20**, 1146.
17. Y. Chen, S.P. Zhao, J.L. Liu, W.H. Ning, X.M. Sun, X.M. Ren, *RSC Adv.* 2014, **4**, 9178.
18. A. Katrusiak and M. Szafrański, *Phys. Rev. Lett.* 1999, **82**, 576.
19. M. Szafrański, A. Katrusiak and G. J. McIntyre, *Phys. Rev. Lett.* 2002, **89**,

215507.

20. A. Budzianowsk and A. Katrusiak, *J. Phys. Chem. B* 2006, **110**, 9755.
21. M. Szafrański, *J. Phys. Chem. B* 2009, **113**, 9479.
22. M. Szafrański and A. Katrusiak, *J. Phys. Chem. B* 2008, **112**, 6779.
23. G. Feguson, C. Glidewell, R.M. Gregson, P.Meehan, I.L.J. Patterson, *Acta Cryst. B* 1998, **54**, 151.
24. *Software packages SMART and SAINT*, Siemens Analytical X-ray Instrument Inc., Madison, WI, 1996.
25. G.M. Sheldrick, *SHELX-97, Program for the refinement of crystal structure*, University of Göttingen, Germany, 1997.
26. M. A. White in Crystal Engineering: *The Design and Application of Functional Solids* (Eds.: K. R. Seddon, M. Zaworotko), Kluwer Acad. Pub., Dordrecht, 1999, 279.
27. R.A. Cowley, *Phys. Rev. B* 1976, **13**, 4877.

Table 1: Crystallographic data and refinement parameters for **1** at 120, 200 and 296 K

Temp. (K)	296	200	120
Wavelength (Å)	0.71073	0.71073	0.71073
Formula	$C_{18}H_{22}N_2O_2$	$C_{18}H_{22}N_2O_2$	$C_{18}H_{22}N_2O_2$
Formula weight	298.38	298.38	298.38
Space group	*C2/c*	*C2/c*	*$P2_1/c$*
CCDC no.	995689	995688	995687
Crystal system	Monoclinic	Monoclinic	Monoclinic
a (Å)	12.1356(18)	11.819(2)	11.3698(18)
b (Å)	6.3400(11)	6.2786(11)	6.2439(9)
c (Å)	21.054(3)	21.136(4)	21.563(3)
β (°)	98.846(5)	97.707(6)	96.206(4)
V(Å^3) / Z	1600.6(4), 4	1554.3(5), 4	1521.8(4), 4
ρ (g·cm^{-1})	1.238	1.275	1.302
F(*000*)	640	640	640
Abs.coeff. (mm^{-1})	0.081	0.084	0.085
θ Range for data collection (°)	1.96 - 25.48	3.48 – 25.50	1.80 – 25.49
Index ranges	-14 ≤ h ≤ 14	-14 ≤ h ≤ 14	-13 ≤ h ≤ 13
	-7 ≤ k ≤ 7	-7 ≤ k ≤ 7	-7 ≤ k ≤ 7
	-22 ≤ l ≤ 25	-23 ≤ l ≤ 25	-24 ≤ l ≤ 26
R_{int}	0.0361	0.0332	0.0393
Independent reflect. /restraints/parameters	1488 / 0 / 138	1436 / 0 / 138	2818 / 0 / 201
Refinement method	The least square refinement on F^2		
Goodness of fit on F^2	1.031	1.048	1.048
R_1, wR_2[a] [$I>2\sigma$(I)]	0.0432, 0.1184	0.0528, 0.1410	0.0444, 0.1063
R_1, wR_2[a] [all data]	0.0588, 0.1257	0.0902, 0.1547	0.0618, 0.1121
Residual (e·Å^{-3})	0.120 / -0.178	0.145 / -0.206	0.170 / -0.254

$R_1 = \sum||F_o| - |F_c||/|F_o|$, $wR_2 = [\sum w(\sum F_o^2 - F_c^2)^2/\sum w(F_o^2)^2]^{1/2}$

Table2: Angles θ1, θ2, and θ3 as well as the geometric parameters of intermolecular H-bonds between DABCO and 4, 4'-biphenol molecules in **1** at 296 K, 200 K, 120 K

Temperature/K	296	200	120
θ1/°	45.5(4)	45.1(4)	46.7(1)
θ2/°	45.5(4)	45.1(4)	43.1(1)
θ3/°	40.3(1)	40.1(1)	39.7(1)
∠O–H…N/°	164.5/166.6	171.2/159.3	169.5/160.3
$d_{O...N}$/Å	2.651(19)/2.771(13)	2.630(19)/2.793(14)	2.686(2)/2.736(2)
$d_{H...N}$/Å	1.852/1.967	1.796/1.991	1.856/1.930

Notes: Two types of H-bonds between OH and N atoms in **1**.

TOC

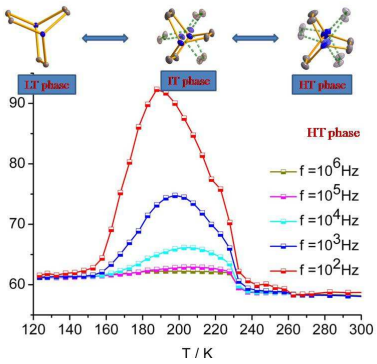

Two-step dielectric anomalies appear in co-crystal of 1,4-diazabicyclo[2.2.2]octane (DABCO) and 4, 4'-biphenol which are coupled with structural phase transitions related to the disorder-order transformation of DABCO molecules.